Bioconjugate Chemistry

Article

pubs.acs.org/bc

Photocontrolled Nuclear-Targeted Drug Delivery by Single Component Photoresponsive Fluorescent Organic Nanoparticles of Acridin-9-Methanol

Avijit Jana,[†,§] Biswajit Saha,[‡] Deb Ranjan Banerjee,[†] Sudip Kumar Ghosh,[‡] Kim Truc Nguyen,[§] Xing Ma,[§] Qiuyu Qu,[§] Yanli Zhao,*[,§,∥] and N. D. Pradeep Singh*[,†]

[†]Department of Chemistry and [‡]Department of Biotechnology, Indian Institute of Technology Kharagpur, Kharagpur 721302, India

[§]Division of Chemistry and Biological Chemistry, School of Physical and Mathematical Sciences, Nanyang Technological University, 21 Nanyang Link, 637371, Singapore

[∥]School of Materials Science and Engineering, Nanyang Technological University, 50 Nanyang Avenue 639798, Singapore

Supporting Information

ABSTRACT: We report for the first time an organic nanoparticle based nuclear-targeted photoresponsive drug delivery system (DDS) for regulated anticancer drug release. Acridin-9-methanol fluorescent organic nanoparticles used in this DDS performed three important roles: (i) "nuclear-targeted nanocarrier" for drug delivery, (ii) "phototrigger" for regulated drug release, and (iii) fluorescent chromophore for cell imaging. In vitro biological studies reveal acridin-9-methanol nanoparticles of ∼60 nm size to be very efficient in delivering the anticancer drug chlorambucil into the target nucleus, killing the cancer cells upon irradiation. Such targeted organic nanoparticles with good biocompatibility, cellular uptake property, and efficient photoregulated drug release ability will be of great benefit in the field of targeted intracellular controlled drug release.

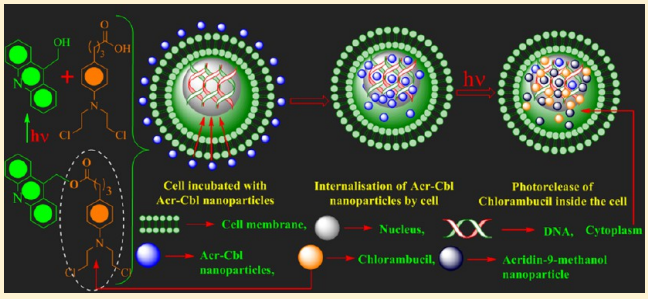

INTRODUCTION

Targeted intracellular drug delivery systems have captured great attention in the medical and pharmaceutical fields, since they sharply enhance the efficiency of various treatment protocols.[1] These targeted drug delivery systems (DDSs) have gained much popularity, especially for tumor therapy, because many anticancer drugs need to be delivered into the cell nucleus, so that they damage the DNA to stop the proliferation of the cell. Hence, several nuclear-targeted intracellular DDSs[2−5] to kill cancer cells have been developed. Among them, nanosized DDSs have gained considerable popularity in recent years.[6−10] A major goal in constructing nuclear-targeted nanosized DDSs is to design nanoparticles that will combine various functionalities, like fluorescence, nuclear-target ability, and precise control over the drug release. To date, several nanoparticles (e.g., magnetic nanoparticles, silver nanoparticles, quantum dots, mesoporous silica, etc.) decorated with nuclear localization signal peptides such as SV40 T antigen,[11] HIV-1 TAT peptide,[12,13] and adenoviral,[14] have been fabricated for nuclear-targeted nano DDSs. However, to the best of our knowledge there has been no report on the construction of nuclear-targeted nanosized DDS using single component nanoparticles that can precisely control the drug release.

Recently, photoresponsive nanoparticles have received much attention for their applications especially in the area of drug[15−25] and gene[26,27] delivery, since they allow precise control over the release including location, timing, and dosage, though most of these photoresponsive nanoparticles fabricated for DDSs have showed enhanced cell permeability. However, to a larger extent these nanoparticles were found to be localized in the cellular membrane or in the cytoplasm. By any means, if we can synthesize nuclear-targeted photoresponsive nanoparticles, then we can aim to develop nuclear-targeted nanosized DDS with precise control over the drug release.

Recently, we demonstrated for the first time that single component photoresponsive nanoparticles can be directly made from a small organic molecule "phototrigger" without attaching with external nanoparticles, for regulated delivery of anticancer drug.[28] Based on the above strategy, we aim to fabricate a new fluorescent organic molecule which has high affinity to DNA and has the ability to act as a phototrigger into single component photoresponsive nanoparticles for nuclear-targeted nanosized DDS, so that the cell imaging, localization of the drug in the cell nucleus, and control over the drug release can be simultaneously accomplished.

Acridine based compounds are planar polycyclic aromatic molecules which bind tightly but reversibly to DNA by intercalation.[29,30] Hence acridine derivatives have been utilized

Received: April 5, 2013
Revised: September 25, 2013
Published: October 22, 2013

dx.doi.org/10.1021/bc400170r | *Bioconjugate Chem.* 2013, 24, 1828−1839

Scheme 1. Schematic Presentation of Photocontrolled Nuclear-Targeted Delivery of Chlorambucil by Photoresponsive Organic Nanoparticles of Acridin-9-Methanol

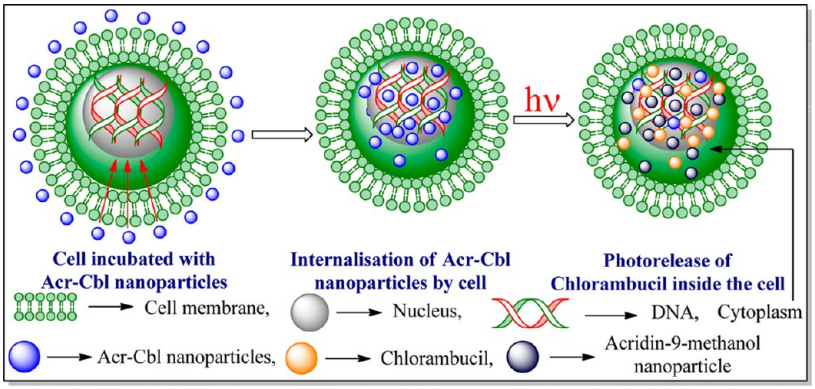

as carriers to target the cell nucleus.[31,32] Mainly, DNA alkylating agents are targeted to DNA by tethering with acridine molecules.[33] On the other hand, a recent report by our group[34a] and by Piloto et al.[34b] showed that acridin-9-ylmethyl chromophore also acts as an efficient phototrigger for amino acids and carboxylic acids. The above properties of acridine moiety to act as both nuclear target and phototrigger led us to develop them as single component fluorescent organic nanoparticles for nuclear-targeted and regulated delivery of anticancer drug (Scheme 1).

MATERIALS AND METHODS

All reagents were purchased from Sigma Aldrich and used without further purification. Acetonitrile and dichloromethane were distilled from CaH_2 before use. ^1H NMR spectra were recorded on a BRUKER-AC 200 MHz spectrometer. Chemical shifts are reported in ppm from tetramethylsilane with the solvent resonance as the internal standard (deuterochloroform: 7.26 ppm). Data are reported as follows: chemical shifts, multiplicity (s = singlet, d = doublet, t = triplet, m = multiplet), coupling constant (Hz). ^{13}C NMR (50 MHz) spectra were recorded on a BRUKER-AC 200 MHz Spectrometer with complete proton decoupling. Chemical shifts are reported in ppm from tetramethylsilane with the solvent resonance as the internal standard (deuterochloroform: 77.0 ppm). UV/vis absorption spectra were recorded on a Shimadzu UV-2450 UV/vis spectrophotometer, fluorescence emission spectra were recorded on a Hitachi F-7000 fluorescence spectrophotometer, FT-IR spectra were recorded on a Perkin-Elmer RXI spectrometer, and HRMS spectra were recorded on a JEOL-AccuTOF JMS-T100L mass spectrometer. Transmission Electron Microscopy (TEM) was measured on a FEI Tecnai G220S-Twin at 200 kV. The TEM sample was prepared by dispersing compounds in water and dropping on the surface of a copper grid. Photolysis of all the ester conjugates were carried out using 125 W medium pressure Hg lamp supplied by SAIC (India). Chromatographic purification was done with 60−120 mesh silica gel (Merck). For reaction monitoring, precoated silica gel 60 F254 TLC sheets (Merck) were used. RP-HPLC was taken using mobile phase acetonitrile, at a flow rate of 1 mL/min (detection: UV 254 nm).

Synthesis of 9-Methylacridine. First, the protecting group 9-methylacridine was synthesized following the procedure as described by Suzuki et al.[35] Treatment of *N,N*-diphenyl amine with glacial acetic acid in the presence of zinc chloride at 215 °C for 6 h afforded the protecting group 9-methylacridine with excellent yield (87%).

A mixture of *N,N*-diphenylamine (6.0g, 36 mmol), acetic acid (6.0 g, 100 mmol), and zinc chloride (25.6 g, 188 mmol) was heated up to 180 °C with continuous stirring for 1 h. Then excess acetic acid was removed from the reaction mixture by distillation and the reaction mixture was heated at 220 °C for additional 5 h followed by addition of aqueous ammonia solution. The resulted yellow precipitates were collected by filtration. The residue was dissolved in chloroform and neutralized by washing with aqueous $NaHCO_3$ and dried over anhydrous Na_2SO_4. The organic solvent was then removed under reduced pressure to give 5.96 g (87%) of crude product, which was further purified by column chromatography using 15% ethyl acetate in pet ether as an eluent.

Characterization data for 9-Methylacridine. Yellow solid, mp: 115−120 °C; ^1H NMR ($CDCl_3$, 200 MHz): δ = 8.14−8.09 (d, J = 8.8 Hz, 2H), 8.09−8.05 (d, J = 8.8 Hz, 2H), 7.69−7.61 (m, 2H), 7.46−7.38 (m, 2H), 2.93 (s, 3H); ^{13}C NMR (CDCl3, 50 MHz): δ = 148.3 (2C), 142.2 (1C), 130.0 (2C), 129.7 (2C), 125.4 (2C), 125.3 (2C), 124.5 (2C), 13.5 (1C).

Synthesis of 9-(Bromomethyl)acridine.[36] 9-Methylacridine (1.00 g, 4.78 mmol) was dissolved in anhydrous CCl_4 and NBS (1.02 g, 5.74 mmol) was added to it followed by catalytic amount of benzoyl peroxide (0.05 g) and the reaction mixture was refluxed for 4 h. The organic compounds were extracted in DCM and washed two times with aqueous $NaHCO_3$ and dried over anhydrous Na_2SO_4. The organic solvent was then removed under reduced pressure to give 1.19 g (92%) of crude product which was used for the protection of chlorambucil without further purification.

Characterization Data for 9-(Bromomethyl)acridine. Yellow solid, mp: 97−99 °C; ^1H NMR ($CDCl_3$, 200 MHz): δ = 8.30−8.27 (d, J = 8.8 Hz, 4H), 7.85−7.77 (m, 2H), 7.72−7.64 (m, 2H), 5.42 (s, 2H); ^{13}C NMR ($CDCl_3$, 50 MHz): δ = 148.7 (2C), 138.6 (1C), 130.4 (2C), 130.0 (2C), 126.6 (2C), 123.7 (2C), 123.3 (2C), 23.1 (1C).

Protection of Chlorambucil with 9-(Bromomethyl)-acridine. 9-(Bromomethyl)acridine (0.100 g, 0.37 mmol) was dissolved in dry dichloromethane (DCM) (2 mL), and to this reaction mixture potassium carbonate (0.061 g, 0.44 mmol) and chlorambucil (0.112 g, 0.37 mmol) were added. The reaction mixture was stirred at room temperature for 6 h. The solvent was removed by rotary evaporation under reduced pressure and the crude residue was purified by column chromatography using 25% EtOAc in pet ether gave compound **3** as a yellow solid (0.159 g, 87%).

Yellow solid; ^1H NMR ($CDCl_3$, 200 MHz): δ = 8.41−8.36 (d, J = 8.8 Hz, 2H), 8.29−8.24 (d, J = 8.8 Hz, 2H), 7.87−7.79

dx.doi.org/10.1021/bc400170r | *Bioconjugate Chem.* 2013, 24, 1828−1839

(t, J = 8.4 Hz, 2H), 7.73−7.65 (t, J = 7.8 Hz, 2H), 7.10−7.06 (d, J = 8.6 Hz, 2H), 6.64−6.60 (d, J = 8.6 Hz, 2H), 5.39 (s, 2H), 3.74−3.57 (m, 8H), 2.63−2.56 (t, J = 7.4 Hz, 2H), 2.43−2.36 (t, J = 7.4 Hz, 2H), 2.01−1.87 (m, 2H); ^{13}C NMR ($CDCl_3$, 50 MHz): δ = 173.7 (1C), 147.6 (2C), 144.4 (1C), 140.8 (1C), 131.1 (2C), 130.6 (1C), 129.7 (2C), 129.2 (2C), 127.1 (2C), 123.9 (2C), 123.5 (2C), 112.3 (2C), 57.6 (1C), 53.7 (2C), 40.6 (2C), 33.9 (1C), 33.4 (1C), 26.6 (1C); FTIR (KBr, cm^{-1}): 1730; UV/vis (EtOH): λ (log ε) 361 (4.07); HRMS calc. for $C_{28}H_{29}Cl_2N_2O_2$ [M+Na$^+$]: 517.1426, found: 517.1420.

Synthesis of Acr-Cbl Nanoparticles. Acridine-Chlorambucil (Acr-Cbl) nanoparticles were synthesized following the reprecipitation technique as described in our earlier report,[28] 10 μL of 3 mM solution of Acr-Cbl caged conjugate in acetone was slowly added into water (20 mL) at room temperature with constant sonication for 30 min. The size of the Acr-Cbl nanoparticles was determined by means of a transmission electron microscopy (TEM).

Synthesis of Acridin-9-Methanol Nanoparticles. Synthesis of acridin-9-methanol nanoparticles was carried out following the same procedure as described in the case of Acr-Cbl nanoparticles.

Hydrolytic Stability of Acr-Cbl Nanoparticles at Different pH Value. One mL of 2 × 10^{-4} M solution of Acr-Cbl nanoparticles was added in PBS solutions (1 mL) of different pH values, and the culture media PBS containing 10% fetal bovine serum with pH = 7.4. All the tubes were kept in ultrasonic for 10 min to make the solutions homogeneous and stored at 37 °C in dark condition for 72 h. Then 2 mL acetonitrile was added to all the tubes and was ultrasonicated for 10 min. Then, all the solutions were centrifuged and the supernatant liquid were analyzed by reverse phase HPLC to examine the remaining percentage of the Acr-Cbl nanoparticles.

Photolysis of Acr-Cbl Nanoparticles Using Visible Light Irradiation (≥410 nm). A suspension of 100 mL of 10^{-4} M of the Acr-Cbl nanoparticles was prepared in water. Half of the suspension was kept in the dark and to the remaining half nitrogen was passed and irradiated using 125 W medium pressure Hg lamp as the light source (≥410 nm) using a suitable filter (1 M $NaNO_2$ solution). At regular time intervals, 0.1 mL of the aliquots was taken and 0.1 mL acetonitrile was added to it, followed by analysis by RP-HPLC using mobile phase acetonitrile, at a flow rate of 1 mL/min (detection: UV 254 nm). Peak areas were determined by RP-HPLC, which indicated gradual decrease of the Acr-Cbl nanoparticles with time, and the average of three runs. The reaction was followed until the consumption of the caged compound is less than 5% of the initial area. Based on HPLC data for each caged compounds, we plotted normalized [A] (HPLC peak area) versus irradiation time. We observed an exponential correlation for the disappearance of the caged compounds which suggested a first order reaction.

Acridin-9-methanol:[37] ^{1}H NMR (DMSO-d^6, 200 MHz): δ = 8.57−8.53 (d, J = 8.8 Hz, 2H), 8.21−8.16 (d, J = 8.6 Hz, 2H), 7.91−7.83, (t, 8.8 Hz, 2H), 7.72−7.64 (t, J = 8.6 Hz, 2H), 5.66 (s, 1H), 5.51 (s, 2H); ^{13}C NMR (DMSO-d^6, 50 MHz): δ = 148.3, 129.9, 129.5, 125.8, 125.3, 124.4, 54.7.

DNA Binding Studies Using Acr-Cbl Nanoparticles with Calf Thymus DNA. *Ethidium Bromide Displacement Assay.* To ascertain the mode of binding of Acr-Cbl nanoparticles to the calf thymus DNA (ct-DNA) competitive EB displacement assay has been performed using Acr-Cbl nanoparticles. Fluorimetric titrations were performed in a 3 cm quartz cuvette using an excitation wavelength of 480 nm. Three mL of 20 μM ct-DNA was saturated with 2 μM of ethidium bromide (EB) solution in 10 mM phosphate buffer pH 7.0 containing 50 mM NaCl. The EBct-DNA solution was then titrated by successive addition of Acr-Cbl nanoparticles to reach a final concentration of ∼38 μM. Emission spectra were recorded from 500 to 750 nm. The fluorescence spectra of EB were measured using an excitation wavelength of 480 nm and the emission range was set between 500 and 750 nm. The spectra were analyzed according to the classical Stern−Volmer eq 1.

$$F_0/F = 1 + K_{sv}[Q] \quad (1)$$

where F_0 and F are the fluorescence intensities in the absence and presence of the quencher, respectively, K_{sv} is the linear Stern−Volmer quenching constant, and [Q] is the concentration of the quencher.

In order to determine the binding constant (K), eq 2[38] was employed.

$$\mathrm{Log}\,\frac{(F_0 - F)}{F} = \mathrm{Log}K + n\mathrm{Log}[Q] \quad (2)$$

where F_0 and F are the fluorescence intensities in the absence and presence of quencher, and [Q] is the concentration of quencher. Log$(F_0 - F)/F$ was plotted against log[Q], and the values of K and n were obtained from the intercept and slope, respectively.

Molecular Docking Study. Molecular docking studies have been carried out to substantiate the intercalation and preferred binding mode of Acr-Cbl caged conjugate with DNA. The crystal structure of DNA was obtained from the Protein Data Bank[39] (PDB entry 3MKY) and was used for the docking studies. The DNA file was prepared for docking by removing water molecules and adding hydrogen atoms with Gasteiger charges. The 3D structure of the ligands was generated in the PRODRG sever[40] and its energy-minimized conformation was obtained using accelrys discovery studio 3.1 by applying CHARMM[41] force field with Momany-Rone partial charges. The rotatable bonds in the ligand were assigned with AutoDock Tools and flexible docking was carried out with Auto Dock 4.2 Lamarckian Genetic Algorithm (GA).[42] The whole DNA was enclosed in a grid having 0.375 Å spacing for blind-docking purposes. Other miscellaneous parameters were assigned the default values given by AutoDock. The output from Auto Dock was rendered in PyMol.[43]

Acr-Cbl Nanoparticles for Cell Imaging Studies Using HeLa Cell Line. Cell imaging studies were carried out using the HeLa cell line obtained from National Centre for Cell Science (NCCS) which was maintained in minimum essential medium (MEM) containing 10% fetal bovine serum (FBS) at 37 °C and 5% CO_2. To study the cellular uptake of Acr-Cbl nanoparticles, briefly HeLa cells (5 × 10^4 cells/well) were plated on 12 well plates and allowed to adhere for 4−8 h. Cells were then incubated with 3 × 10^{-5} M, both the compounds separately in cell culture medium for 4 h at 37 °C and 5% CO_2. Thereafter, cells were fixed in paraformaldehyde for 15 min and washed two times with PBS. Imaging was done in Olympus confocal microscope (FV1000, Olympus) using the respective filter.

Nuclear Co-Localization Studies Using Acr-Cbl Nanoparticles and a Nuclear Staining Dye Propidium Iodide. Cells, grown and plated as described above, were incubated for 4 h at 37 °C with 1 mL of MEM containing 20 μM of Acr-Cbl nanoparticles. Thereafter, cells were washed 3 times with 10 mM PBS and fixed with 2% paraformaldehyde for 15 min at room temperature. After fixation cells were washed 3 times with 10 mM PBS permiabilized with 0.01% Triton X 100, a nonionic

surfactant. The cells were counterstained with 10 μg/mL propidium iodide (PI) and 0.5 μg/mL RNASE at room temperature in the dark for 30 min. After gentle washing in 10 mM PBS 3 times, the cells were viewed under confocal microscope.

Cytotoxicity of Acridin-9-Methanol Nanoparticles and the Acr-Cbl Nanoparticles on HeLa Cell Line. Cytotoxicity before Photolysis. The cytotoxicity in vitro was measured using the MTT (3-(4,5-dimethylthiazol-2-yl)-2,5-diphenyltetrazolium bromide, a yellow tetrazole) assay on HeLa cell line. Briefly, cells growing in log phase were seeded into 96-well cell-culture plate at 1×10^4 cells/mL. Different concentration of Acr-Cbl nanoparticles, acridin-9-methanol nanoparticle, and chloambucil were added into the wells with an equal volume of PBS in the control wells. The cells were then incubated for 72 h at 37 °C in 5% CO_2. Thereafter, fresh media containing 0.40 mg/mL MTT were added to the 95 well plates and incubated for 4 h at 37 °C in 5% CO_2. Formazan crystals thus formed were dissolved in DMSO after decanting the earlier media and absorbance recorded at 595 nm.

Cytotoxicity after Photolysis. HeLa cells maintained in minimum essential medium (in 96-well cell-culture plate at concentration of 1×10^4 cells/mL) containing 10% fetal bovine serum (FBS) and different concentrations (0.5, 1, 5, 10, 15, and 20 μM) of Acr-Cbl nanoparticles, acridin-9-methanol nanoparticle, and chloambucil were incubated for 4 h at 37 °C and 5% CO_2. Then the cells were irradiated (keeping the cell-culture plate 5 cm apart from the light source) using 125 W medium pressure Hg lamp as irradiation source (≥410 nm) and 1 M $NaNO_2$ solution as UV cutoff filter. After irradiation the cells were again incubated for 72 h. Then, cytotoxicity was measured using the MTT assay as described in the previous section.

Cell Apoptosis Studies. To study the cell apoptosis induced by of Acr-Cbl nanoparticles, briefly HeLa cells (5×10^4 cells/well) were plated on 6 well plates and allowed to adhere for 8 h. Cells were then incubated with 3×10^{-5} M Acr-Cbl nanoparticles in cell culture medium for 4 h at 37 °C and 5% CO_2, then irradiated for 30 min, and then the cells were incubated for another 24 h at 37 °C and 5% CO_2. Thereafter, cells were washed two times with PBS and were collected by centrifuging. Then, cells were resuspended in annexin-binding buffer and were deposited on a glass slide followed by 5 μL of Annexin V and 2 μL of PI solutions were added and were incubated for another 15 min. Imaging was done in Olympus confocal microscope (FV1000, Olympus) using the respective filter.

Scheme 2. Synthesis of Photocaged Acridine-Chlorambucil (Acr-Cbl) Conjugate

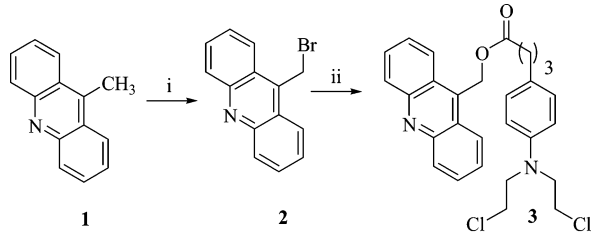

Regeants and conditions: i) NBS, $(PhCO)_2O_2$, CCl_4 reflux, ii) Chlorambucil, K_2CO_3, DCM, rt

RESULTS AND DISCUSSION

Synthesis of Acridine-Chlorambucil (Acr-Cbl) Conjugate. First, we synthesized a photocaged Acridine-Chlorambucil (Acr-Cbl) conjugate as shown in Scheme 2. Bromination of 9-methylacridine in the presence of *N*-bromosuccinimide (NBS) afforded compound **2**, which on treatment with anticancer drug chlorambucil in the presence of K_2CO_3 in dry DCM yielded the final photocaged product **3**.

Synthesis and Characterization of Acr-Cbl and Acridin-9-Methanol Nanoparticles. Next, we synthesized Acr-Cbl nanoparticles for DDS following the reprecipitation technique by the means of slow addition of 5 μL of 3 mM acetone solution of Acr-Cbl caged conjugate into 25 mL water with constant sonication for 30 min. By using similar reprecipitation technique, phototrigger acridin-9-methanol nanoparticles were also synthesized. The size of the resulting nanoparticles of Acr-Cbl and acridin-9-methanol were determined by transmission electron microscopy (TEM), and it was found that both the Acr-Cbl as well as acridin-9-methanol nanoparticles are spherical in shape and the average particle size is of 60 nm (Figure 1a–b) and 55 nm, respectively (Figure 1d). We also have measured the surface charge of Acr-Cbl nanoparticles by measuring the zeta potential at neutral pH. The Acr-Cbl nano particles revealed a zeta potential of about −19.3 mV at neutral pH, which suggests that the aqueous dispersion of Acr-Cbl nanoparticles is sufficiently stable for in vitro delivery of the anticancer drug.

The absorption spectra of Acr-Cbl nanoparticles were found to be quite different compared to acridin-9-methanol nanoparticles, but their emission spectra resembled each other (Figure 2). The broad absorbance of the Acr-Cbl nanoparticles from 330 to 500 nm and strong emission at 480 nm indicates that Acr-Cbl nanoparticles can be used both for cell imaging and for the

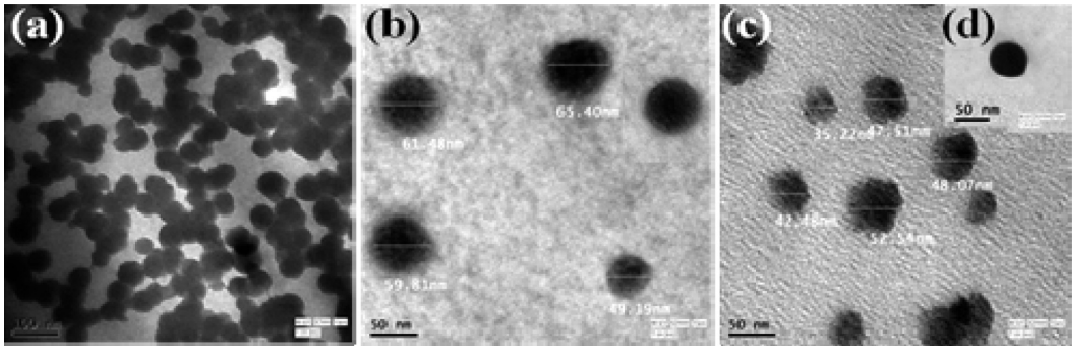

Figure 1. (a–d) TEM images of (a,b) Acr-Cbl nanoparticles before photolysis, (c) Acr-Cbl nanoparticles after photolysis, (d) TEM image of acridin-9-methanol nanoparticles.

dx.doi.org/10.1021/bc400170r | *Bioconjugate Chem.* 2013, 24, 1828–1839

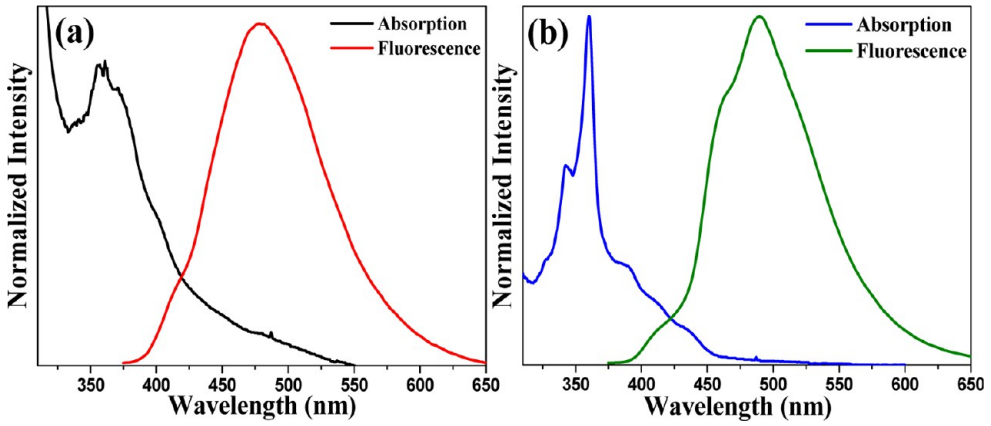

Figure 2. (a–b) Normalized absorption and emission spectra: (a) Acr-Cbl nanoparticles, (b) acridin-9-methanol nanoparticles.

Table 1. Remaining Percentages of Acr-Cbl Conjugate in Dark Condition at Different pH Values

		hydrolytical stability data Acr-Cbl conjugate			
substrate	time (h)	% of depleted[a](pH 5.6) PBS	% of depleted[a](pH 7.4) PBS	% of depleted[a](pH 8) PBS	% of depleted[a](pH 7.4) 10%FBS
Acr-Cbl nanoparticles	72	4	5	5	3
Acr-Cbl nonagregated	72	12	8	21	7

[a]As determined by reverse phase HPLC.

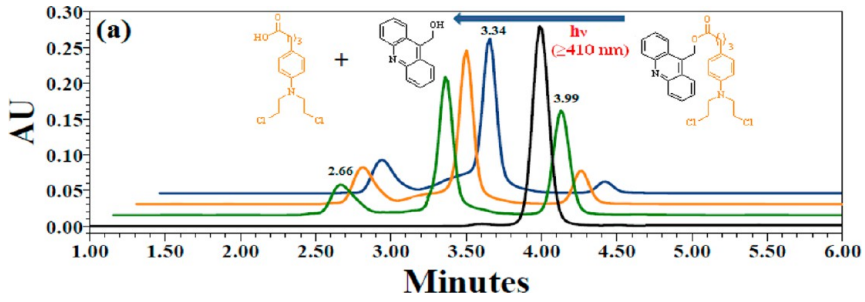

Figure 3. HPLC profile for the pprogress of the release of chlorambucil from Acr-Cbl nanoparticles using visible light (≥410 nm) irradiation (*X* axis is offset by 10 s and the *Y* axis is offset by 10 mAU for better visualization).

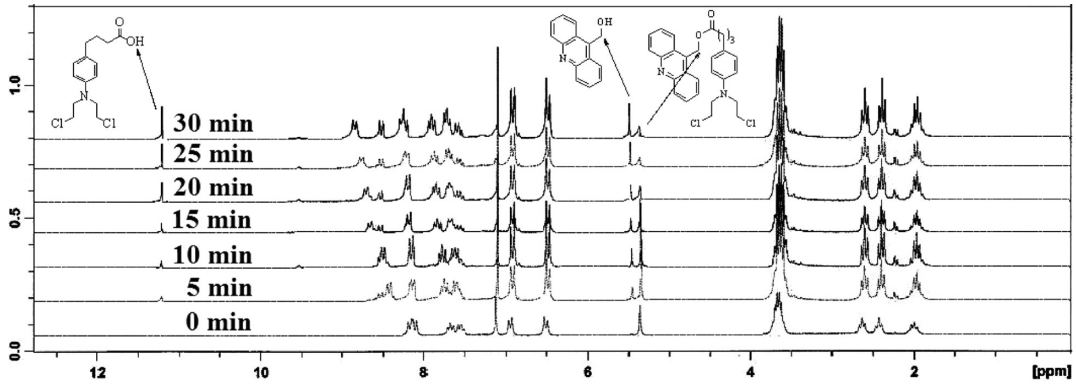

Figure 4. ^{1}H NMR spectral profile of caged chlorambucil at different irradiation times.

release of anticancer drug under soft visible light irradiation (≥410 nm).

Hydrolytic Stability of Acr-Cbl Conjugate at Different pH Value. To check the hydrolytic stability of Acr-Cbl nanoparticles, 1 mL of PBS solution containing 2×10^{-4} M of Acr-Cbl nanoparticles at different initial pH values (5.6, 7.4, and 8) was prepared, separately. On the other hand, the culture media PBS containing 10% fetal bovine serum at pH = 7.4 was also prepared to monitor the stability of Acr-Cbl nanoparticles under the biological environment. All the tubes were kept in ultrasonic for 10 min to make the solutions homogeneous and stored at 37 °C in dark condition for 72 h. Then 2 mL acetonitrile was added to all the tubes and was ultrasonicated for 10 min. Then all the solutions were centrifuged and the supernatant liquid were analyzed by reverse phase HPLC to examine the remaining percentage of the Acr-Cbl conjugates. We observed insignificant (3–5%) decomposition (Table 1) of the Acr-Cbl nanoparticles under dark condition (data given is the average

dx.doi.org/10.1021/bc400170r | *Bioconjugate Chem.* 2013, 24, 1828–1839

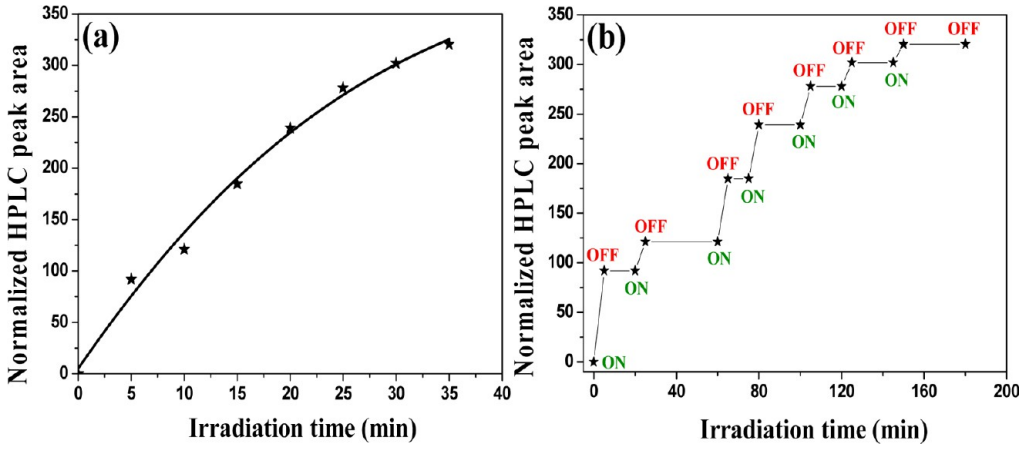

Figure 5. (a) Time course for the photorelease of chlorambucil from Acr-Cbl nanoparticles under visible light irradiation (≥410 nm). (b) Progress of release of chlorambucil under bright and dark conditions. "On" indicates the beginning of light irradiation and "OFF" indicates the ending of light irradiation.

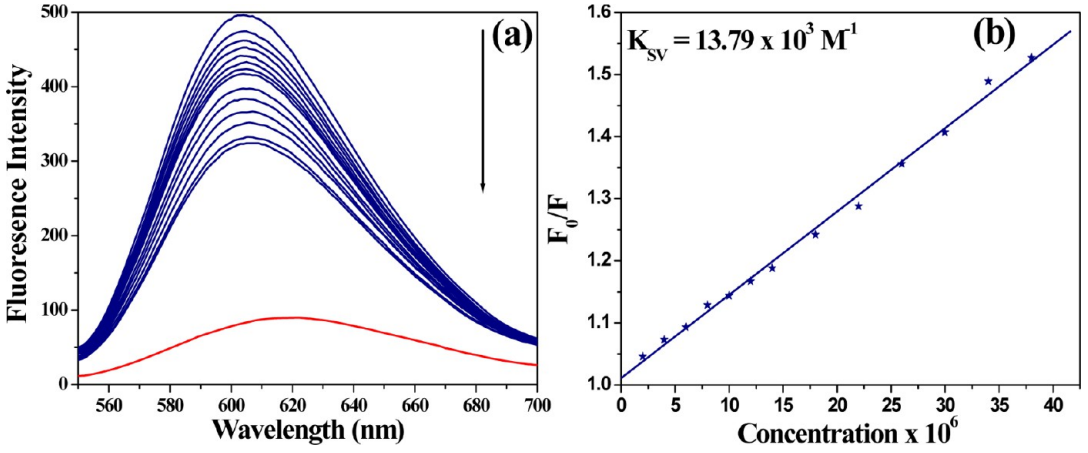

Figure 6. (a) Fluorescence quenching spectra of EB-ct-DNA with Acr-Cbl nanoparticles. The red line indicates the fluorescence emission spectra of EB in the absence of ct-DNA and the top blue line indicates the fluorescence emission spectra of EB bound to ct-DNA; [EB] = 2 μM, [ct-DNA] = 20 μM, [Acr-Cbl nanoparticles] = 0−38 μM. (b) The quenching of EB bound to ct-DNA by Acr-Cbl nanoparticles is in good agreement with the linear Stern−Volmer equation.

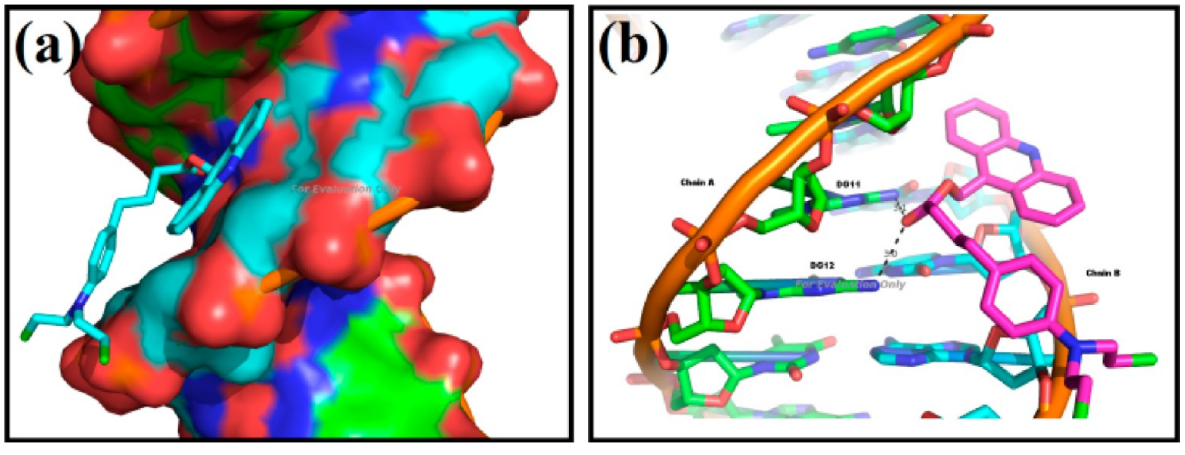

Figure 7. Docked conformations of DNA-Acr-Cbl caged conjugate (a) surface representation showing the binding pockets of conjugate; (b) stereoview of the docked conformations of Acr-Cbl conjugate showing that the ester carbonyl is forming H-bond with guanine N7 H-atom thereby facilitating DNA-alkylation.

of three parallel experiments) which proves that the Acr-Cbl nanoparticles are quite stable under the dark condition. When the similar experiment was carried out with nonaggregated Acr-Cbl conjugate, a slightly higher extent of decomposition (7−21%) of the Acr-Cbl was observed (Table 1).

Further, the stability of the aqueous suspension of Acr-Cbl nanoparticles was tested by recording the emission spectra of aqueous dispersion of Acr-Cbl nanoparticles for consecutive 7 days, and we observed that the emission spectra remain almost unaltered (Supporting Information, Figure S1) even after 7 days,

dx.doi.org/10.1021/bc400170r | *Bioconjugate Chem.* 2013, 24, 1828−1839

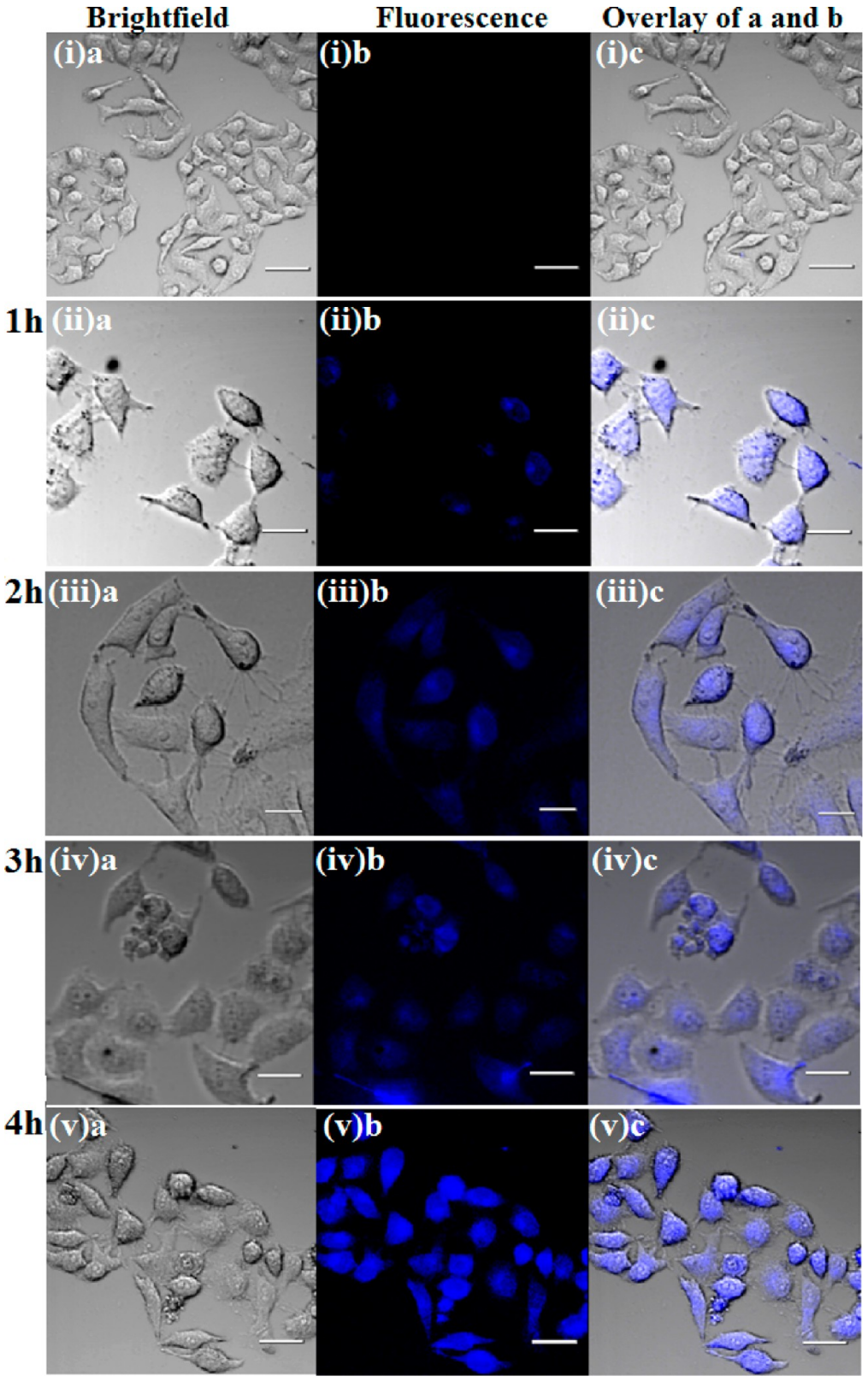

Figure 8. Confocal fluorescence and brightfield images of HeLa cells: (i) untreated cells; (ii–v) cells + Acr-Cbl nanoparticles (4×10^{-5} M): (ii) after 1 h, (iii) after 2 h, (iv) after 3 h, and (v) after 4 h of incubation (Scale bar = 20 μm).

which means the aqueous dispersion of Acr-Cbl nanoparticles is stable enough to be used as DDS.

Photoinduced Release of Chlorambucil from Acr-Cbl Nanoparticles. A suspension of the Acr-Cbl nanoparticles in water (1×10^{-4} M) was irradiated under visible light (≥410 nm) by 125 W medium pressure Hg lamp using a suitable filter (1 M $NaNO_2$ solution) and the course of the photorelease was followed by reverse phase HPLC. A known amount of aqueous

dx.doi.org/10.1021/bc400170r | *Bioconjugate Chem.* 2013, 24, 1828–1839

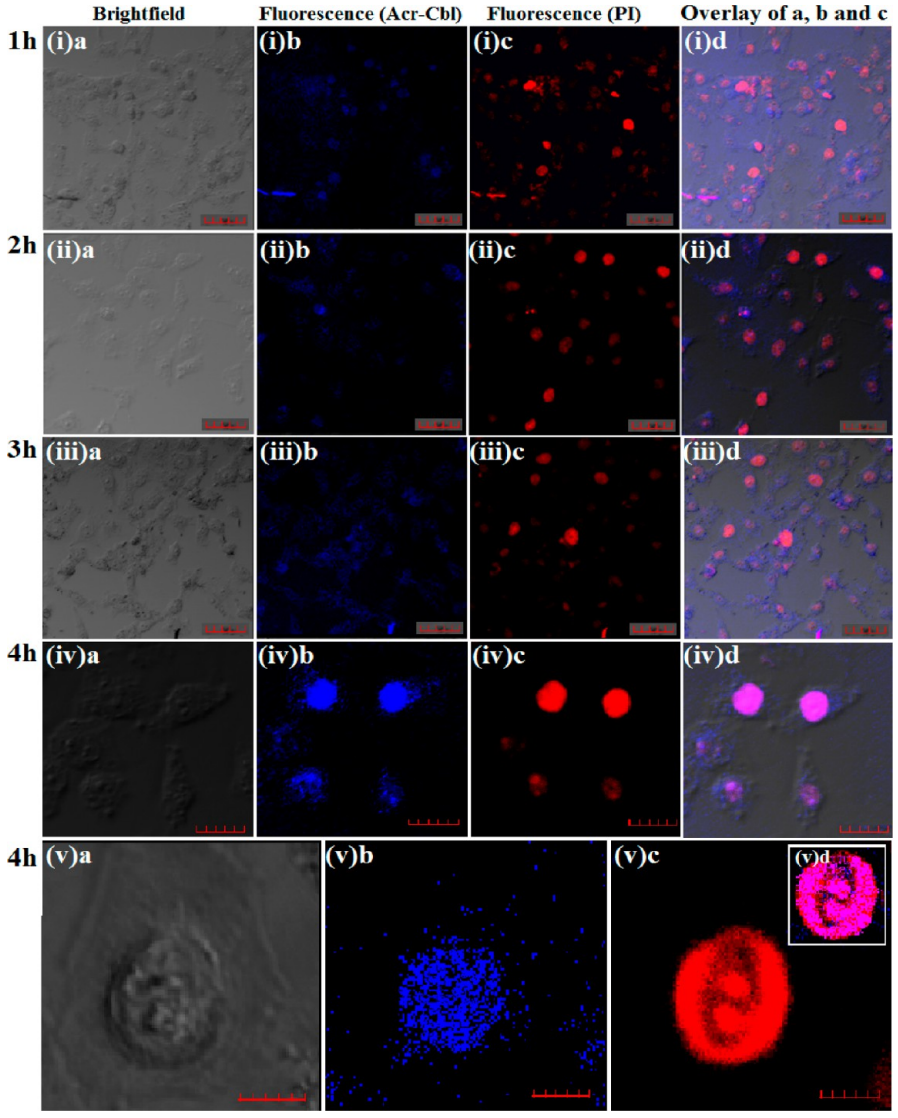

Figure 9. Confocal fluorescence and brightfield images of HeLa cells: (i–v) Cells were incubated with 20 μM Acr-Cbl nanoparticles for different time intervals (1–4 h) followed by fixation of cells and nuclear staining by PI, (a) brightfield image of cells, (b) showing the uptake of Acr-Cbl nanoparticles (λ_{ex} = 410 nm), (c) showing the uptake of PI (25 nM, λ_{ex} = 535 nm), (d) overlay image of a, b, and c, which shows that both Acr-Cbl nanoparticles and PI are located at the cell nuclei, (v)a–c: Image of a treated single HeLa cell showing the accumulation of Acr-Cbl nanoparticles inside the HeLa cell. (v)d: showing the profound accumulation of both Acr-Cbl nanoparticles and PI in the HeLa cell nuclei (violet color). The blue fluorescence is from Acr-Cbl nanoparticles and the red fluorescence is from PI used to stain the nuclei. (Scale bar = 20 μm.)

suspension of the photolysate (0.1 mL) was taken at regular intervals of time and subjected to reverse phase HPLC. HPLC profile (Figure 3) showed a clean photocleavage of the Acr-Cbl conjugate into corresponding photoproduct chlorambucil and acridin-9-methanol.

We also have followed the course of the photorelease by ^{1}H NMR spectroscopy. A known amount (1 mL) of aqueous suspension of the photolysate was taken at regular intervals of time and was extracted in dichloromethane (DCM), then solvent was evaporated under vacuum and redissolved in $CDCl_3$ and the ^{1}H NMR was recorded. ^{1}H NMR spectra showed a clean photocleavage of the Acridine-Cbl conjugate into corresponding photoproduct chlorambucil and acridin-9-methanol (Figure 4).

The course of the photorelease of the anticancer drug was then quantified by plotting the HPLC peak area obtained for chlorambucil (Figure 5a). The reaction was followed until the consumption of the Acr-Cbl nanoparticles is less than 5% of the initial area. We also established precise control over the photolytic release of the anticancer drug by monitoring the release of chlorambucil after periods of exposure to light and dark condition as shown in the Figure 5b. From the figure it can be clearly seen that the drug release proceeds only under illumination.

DNA Binding Studies Using Acr-Cbl Nanoparticles. Ethidium bromide displacement assay: To ascertain the mode of binding of Acr-Cbl nanoparticles to the calf thymus DNA (ct-DNA), competitive EB displacement assay was performed using Acr-Cbl nanoparticles. Initially the fluorescence intensity of ethidium bromide (EB), a well-known classical intercalator, was enhanced upon complexation with the DNA. But later on, addition of increasing concentration of Acr-Cbl nanoparticles to EB bound DNA, and the fluorescence intensity of EB gradually decreased (Figure 6a), indicating that Acr-Cbl nanoparticles preferred to bind DNA in an intercalative manner. Further, the affinity constant of Acr-Cbl nanoparticles was found to be 1.59×10^6 M^{-1} which is similar to that of other strong acridine DNA binders.[44,45]

dx.doi.org/10.1021/bc400170r | Bioconjugate Chem. 2013, 24, 1828–1839

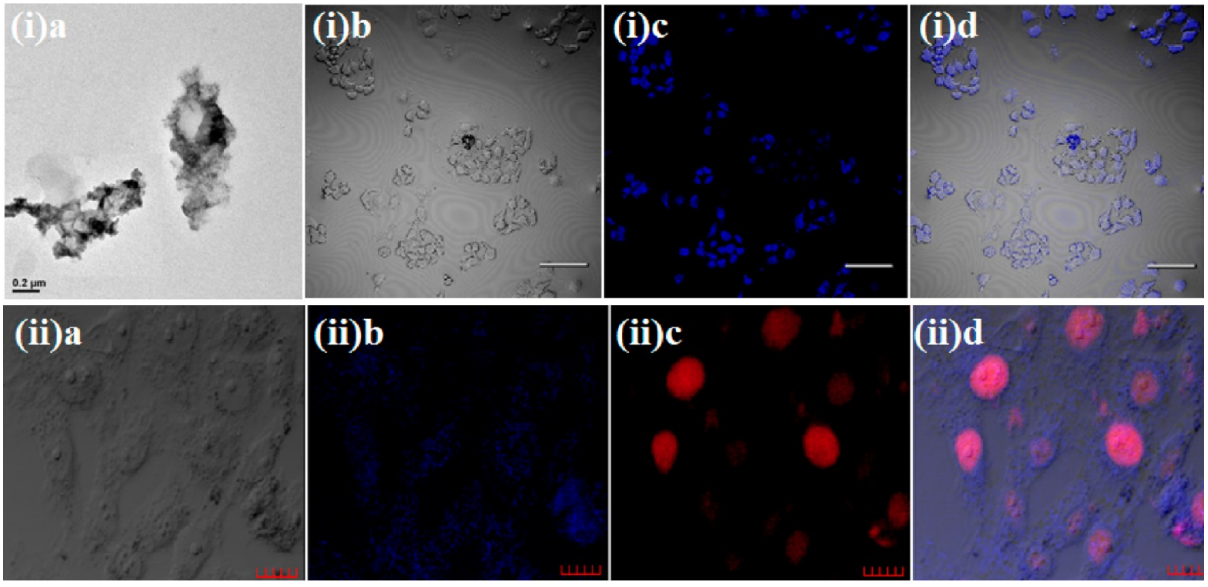

Figure 10. (i)a: TEM image of nonaggregated Acr-Cbl. (1b–iid) Confocal fluorescence and brightfield images of HeLa cells: (ib–d) cells + nonaggregated Acr-Cbl (4×10^{-5} M) after 4 h of incubation: (ib) brightfield image, (ic) fluorescence image and (id) overlay image of ib and ic, (i–v) Cells were incubated with 20 μM Acr-Cbl nanoparticles.

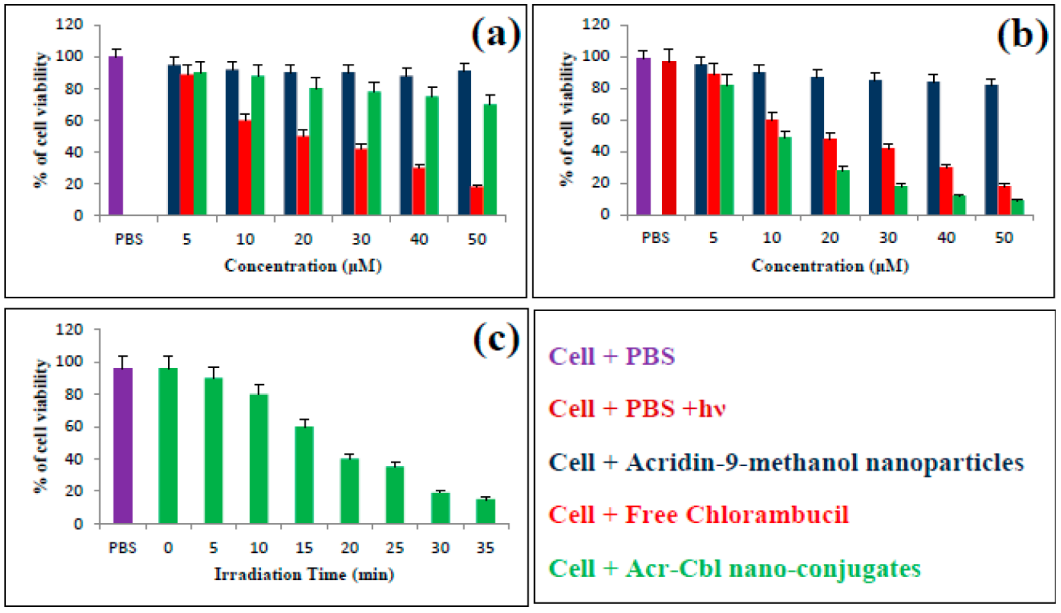

Figure 11. (a–b) Cell viability test of Acr-Cbl nanoparticles, acridin-9-methanol nanoparticles and chlorambucil in HeLa cell line: (a) before irradiation, (b) after irradiation; and (c) cell viability test at regular time intervals of irradiation in the presence of 3×10^{-5} M Acr-Cbl nanoparticles. Values are presented as mean ± SD.

Molecular Docking Studies Using Acr-Cbl Caged Conjugate. To substantiate the intercalation and preferred binding mode of the prodrug Acr-Cbl conjugate with DNA, we performed molecular docking studies. The docking study corroborates the experimental findings, which suggest that Acr-Cbl conjugates are behaving as DNA-intercalators. The docking analysis reveals that the planar acridine moiety of Acr-Cbl caged conjugates acts as a minor groove binder (Figure 7a) whereas the ester carbonyl group forms hydrogen bonds with two guanine N7–H atom as reflected in the Figure 7b. Therefore, the acridine moiety acts as the carrier for the anticancer drug chlorambucil, whereas the H-bonding of the carbonyl group with guanine N7–H atom indicates that DNA alkylation might proceed through guanine efficiently after the release of chlorambucil.

Cellular Uptake Studies of Acr-Cbl Nanoparticles. To investigate real-time cellular uptake property of Acr-Cbl nanoparticles, we carried out cell imaging studies using the cancerous HeLa cell line, which was obtained from the National Centre for Cell Sciences, Pune (NCCS). HeLa cell line was maintained in minimum essential medium containing 10% fetal bovine serum at 37 °C and 5% CO_2. HeLa cells (5×10^4 cells/well) were plated on 12 well plates and allowed to adhere for 4–8 h. Cells were then incubated with 4×10^{-5} M of Acr-Cbl nanoparticles in cell culture medium for different time intervals (1–4 h) at 37 °C and 5% CO_2. Thereafter, cells were fixed in 2% paraformaldehyde for

dx.doi.org/10.1021/bc400170r | Bioconjugate Chem. 2013, 24, 1828–1839

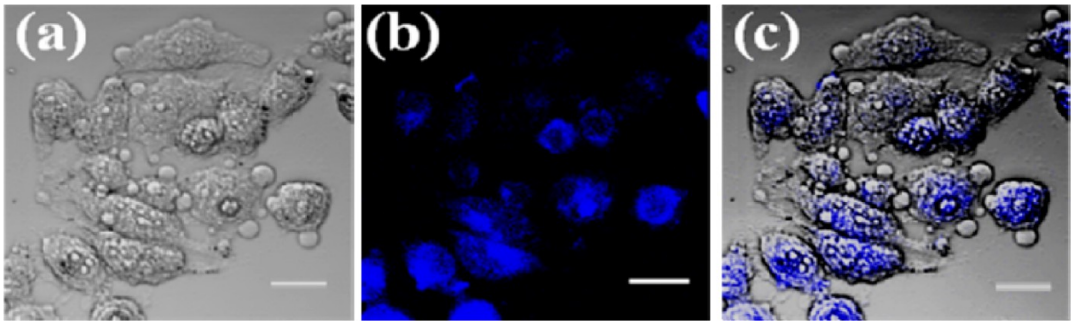

Figure 12. Confocal fluorescence and brightfield images of HeLa cells Acr-Cbl nanoparticles (4×10^{-5} M) + 35 min irradiation (a) brightfield, (b) fluorescence (λ_{ex} 410 nm), and (c) overlay image of a and b. (Scale bar = 20 μm.)

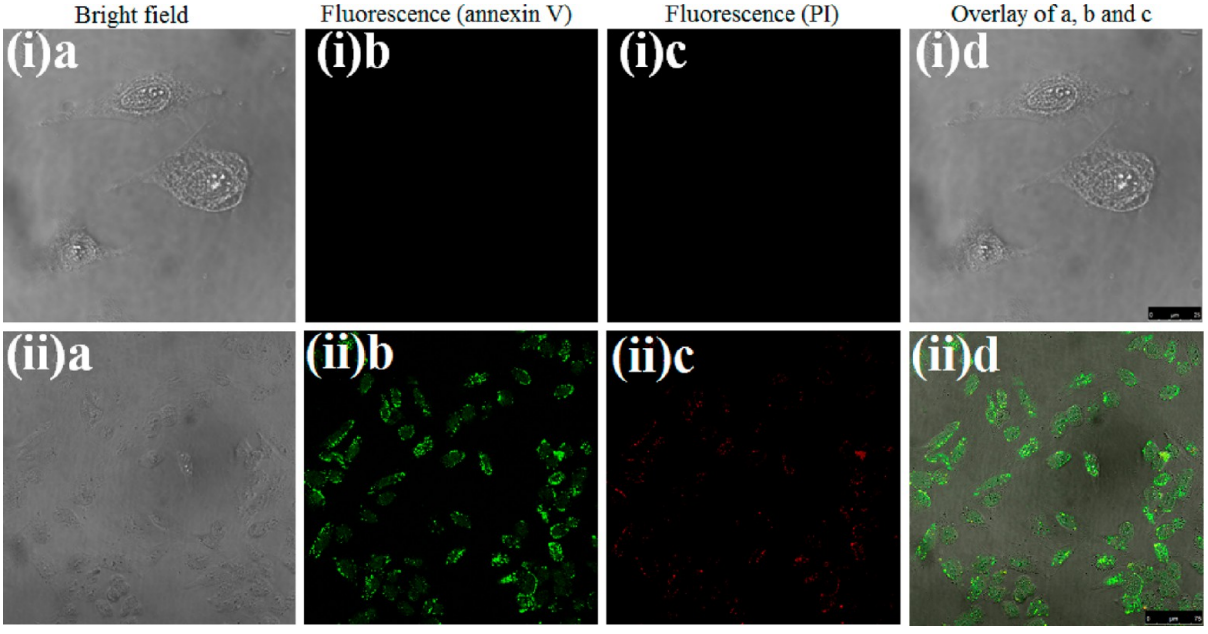

Figure 13. Confocal fluorescence and brightfield images of HeLa cells: (ia-d) untreated cells, (iia-d) cells + Acr-Cbl nanoparticles (4×10^{-5} M), + 35 min irradiation followed by staining with annexin V and PI (propidium iodide). (Scale bar = 25 and 75 μm, respectively.)

15 min and washed two times with PBS. Imaging was done with Olympus confocal microscope (FV1000, Olympus) using the respective filter. Cellular uptake study after 1−4 h incubation reveals that the Acr-Cbl nanoparticles were internalized by the cell membrane in increasing concentration with the increase of exposure time, and the maximum accumulation of Acr-Cbl nanoparticles at the cell nucleus was observed after 4 h of exposure as detected by confocal microscopy (Figure 8).

Further, to study the localization of the Acr-Cbl nanoparticles inside the HeLa cell, we stained the cell nuclei with propidium iodide. After exposing the HeLa cells to Acr-Cbl nanoparticles for different time intervals, followed by propidium iodide, we noted that nanoparticles were readily internalized by the cell membrane and found to be located in the cell nucleus in increasing concentration with the increase of exposure time, and the maximum accumulation of Acr-Cbl nanoparticles at the cell nucleus was observed after 4 h of exposure as detected by confocal microscopy (Figure 9).

Cellular Uptake Studies of Nonaggregated Acr-Cbl Conjugate. To investigate whether the aggregation of Acr-Cbl conjugate is inducing any advantage over the nonaggregated Acr-Cbl conjugate, the cell imaging studies were carried out using the nonaggregated Acr-Cbl conjugate following similar experimental procedure to that of Acr-Cbl nanoparticles. From Figure 10(ib-d), it can be seen that the nonaggregated Acr-Cbl conjugate is readily internalized by the cell membrane, but when we carried out nuclear colocalization studies using propidium iodide, we noted that the Acr-Cbl conjugate is mostly located in the cytoplasm along with the trivial accumulation in the nucleus (Figure 10(iib-d)). Thus, aggregation of Acr-Cbl conjugate into nanoparticles plays an important role in its profound accumulation in the cell nucleus.

Anticancer Efficacy of Acr-Cbl Nanoparticles before and after Photolysis. After successful demonstration of pronounced accumulation of Acr-Cbl nanoparticles within the nucleus of HeLa cells, we evaluated the cytotoxicity of Acr-Cbl nanoparticles, chlorambucil, and acridin-9-methanol nanoparticles *in vitro* using the MTT (3-(4,5-dimethylthiazol-2-yl)-2,5-diphenyltetrazolium bromide a yellow tetrazole) assay in HeLa cell line. Briefly, HeLa cells in their exponential growth phase were trypsinized and seeded into 96-well cell-culture plate at the density of 1×10^4 cells/mL in 100 μL DMEM complete medium. Different concentrations of Acr-Cbl nanoparticles, chlorambucil, and acridin-9-methanol nanoparticles were added in the wells with an equal volume of PBS in the control wells. The cells were then incubated for 72 h at 37 °C in 5% CO_2. Later, fresh media containing 0.40 mg/mL MTT were added to the above 96-well plates and incubated at 37 °C for additional 4 h. Thereafter, the medium was removed, the formazan

dx.doi.org/10.1021/bc400170r | *Bioconjugate Chem.* 2013, 24, 1828−1839

crystals formed were dissolved in DMSO, and the absorbance was recorded at 595 nm. It was observed that cell viability remains above 90% at different concentrations of Acr-Cbl nanoparticles and acridin-9-methanol nanoparticles, whereas an increasing cytotoxicity was observed on addition of increasing amount of chlorambucil (Figure 11a).

For the light exposure experiment, cells incubated with different concentrations of Acr-Cbl nanoparticles on irradiation for 35 min under visible light (≥410 nm) resulted in the release of the anticancer drug chlorambucil, thereby causing cytotoxicity in cancerous HeLa cell lines as validated by the MTT toxicity data (Figure 11b and c) and the apoptosis of HeLa cell line was further confirmed by cellular imaging studies (Figure 12).

On the other hand, there was no significant cell death observed when the cells were irradiated in the presence of acridin-9-methanol nanoparticles or in the absence of Acr-Cbl nanoparticles, indicating that cytotoxicity was likely caused by the released drug, chlorambucil, upon light irradiation. On comparison with the same concentration of chlorambucil to that of Acr-Cbl nanoparticles (Figure 11a), Acr-Cbl nanoparticles showed much lower cytotoxicity compared to chlorambucil. But upon irradiation, Acr-Cbl nanoparticles showed an enhanced cytotoxicity (Figure 11b and c) to cancer cells in comparison to chlorambucil, because of the efficient photorelease of chlorambucil inside the cell nucleus. Thus, the Acr-Cbl nanoparticles serve as a versatile nanosized DDS for the release of the anticancer drug inside the cell nucleus.

Further, to investigate whether the killing of cancerous HeLa cell by the means of photorelease of chlorambucil from Acr-Cbl nanoparticles proceeds through apoptosis or necrosis, we carried out annexin V and PI (propedium iodide) staining experiment using the Alexa Fluor 488 annexin V/Dead Cell Apoptosis Kit. After staining with annexin V and PI, on confocal fluorescence imaging it was observed that the cell membrane of most of the HeLa cells are being stained with annexin V (Figure 13iib, green fluorescent) but the cell nuclei were not stained with propidium iodide (Figure 13iic), which means the cell death proceeds through apoptosis, not by the necrosis pathway.

CONCLUSIONS

In summary, we have developed excellent single component photoresponsive organic nanoparticles made of acridin-9-methanol for photocontrolled nuclear-targeted delivery of anticancer drug. The strong fluorescence of acridin-9-methanol nanoparticles has been explored for the *in vitro* cellular imaging application. Photoregulated drug release ability of acridin-9-methanol nanoparticles has been established by means of periodic exposure to light and dark condition. Importantly, acridin-9-methanol nanoparticles facilitated the active nuclear entry of anticancer drug chlorambucil. Further light irradiation enhanced cytotoxicity of Acr-Cbl nanoparticles compared to free drug against HeLa cells. Finally, though our photoresponsive organic nanoparticles are effective for targeted and regulated drug delivery, their application toward in vivo studies is still restricted due to their absorption below 500 nm. Hence, in the future we would like to design photoresponsive organic nanoparticles which can be operated in the NIR region.

ASSOCIATED CONTENT

Supporting Information

Synthesis details, characterization data, and other experimental details. This material is available free of charge via the Internet at http://pubs.acs.org.

AUTHOR INFORMATION

Corresponding Author

*E-mail: ndpradeep@chem.iitkgp.ernet.in; zhaoyanli@ntu.edu.sg.

Author Contributions

The manuscript was written through contributions of all authors. All authors have given approval to the final version of the manuscript.

Notes

The authors declare no competing financial interest.

ACKNOWLEDGMENTS

DST−FIST for 400 MHz NMR and Confocal Microscope facility. Avijit Jana is thankful to CSIR and Biswajit Saha to DBT for their fellowship. Yanli Zhao thanks financial support from the Singapore National Research Foundation Fellowship (NRF2009NRFRF001-015).

ABBREVIATIONS

Acr, Acridine; Cbl, Chlorambucil; TLC, thin layer chromatography

REFERENCES

(1) Torchilin, V. P. (2006) Recent approaches to intracellular delivery of drugs and DNA and organelle targeting. *Annu. Rev. Biomed. Eng. 8*, 343−375.

(2) Austin, L. A., Kang, B., Yen, C. W., and El-Sayed, M. A. (2011) Nuclear targeted silver nanospheres perturb the cancer cell cycle differently than those of nanogold. *Bioconjugate Chem. 22*, 2324−2331.

(3) Austin, L. A., Kang, B., Yen, C. W., and El-Sayed, M. A. (2011) Plasmonic imaging of human oral cancer cell communities during programmed cell death by nuclear-targeting silver nanoparticles. *J. Am. Chem. Soc. 133*, 17594−17597.

(4) Chen, F., and Gerion, D. (2004) Fluorescent CdSe/ZnS nanocrystal-peptide conjugates for long-term, nontoxic imaging and nuclear targeting in living cells. *Nano Lett. 4*, 1827−1832.

(5) Xu, C., Xie, J., Kohler, N., Walsh, E. G., Chin, Y. E., and Sun, S. (2008) Monodisperse magnetite nanoparticles coupled with nuclear localization signal peptide for cell-nucleus targeting. *Chem. Asian J. 3*, 548−552.

(6) Chen, Y., Chen, H., Zhang, S., Chen, F., Zhang, L., Zhang, J., Zhu, M., Wu, H., Guo, L., Feng, J., and Shi, J. (2011) Multifunctional mesoporous nanoellipsoids for biological bimodal imaging and magnetically targeted delivery of anticancer drugs. *Adv. Funct. Mater. 21*, 270−278.

(7) Wu, H., Zhang, S., Zhang, J., Liu, G., Shi, J., Zhang, L., Cui, X., Ruan, M., He, Q., and Bu, W. A (2011) Hollow-core, magnetic, and mesoporous double-shell nanostructure: in situ decomposition/reduction synthesis, bioimaging, and drug-delivery properties. *Adv. Funct. Mater. 21*, 1850−1862.

(8) Du, J. Z., Du, X. J., Mao, C. Q., and Wang, J. (2011) Tailor-made dual pH-sensitive polymer-doxorubicin nanoparticles for efficient anticancer drug delivery. *J. Am. Chem. Soc. 133*, 17560−17563.

(9) Zhang, Q., Liu, F., Nguyen, K. T., Ma, X., Wang, X., Xing, B., and Zhao, Y. (2012) Multifunctional mesoporous silica nanoparticles for cancer-targeted and controlled drug delivery. *Adv. Funct. Mater. 22*, 5144−5156.

(10) Yan, H., Teh, C., Sreejith, S., Zhu, L., Kwok, A., Fang, W., Ma, X., Nguyen, K. T., Korzh, V., and Zhao, Y. (2012) Functional mesoporous silica nanoparticles for photothermal-controlled drug delivery in vivo. *Angew. Chem., Int. Ed. 51*, 8373−8377.

(11) Tkachenko, G., Xie, H., Coleman, D., Glomm, W., Ryan, J., Anderson, M. F., Franzen, S., and Feldheim, D. L. (2003) Multifunctional gold nanoparticle-peptide complexes for nuclear targeting. *J. Am. Chem. Soc. 125*, 4700−4701.

(12) Lin, S., Chen, N., Sun, S., Chang, J., Wang, Y., Yang, C., and Lo, L. (2010) The protease-mediated nucleus shuttles of subnanometer gold

quantum dots for real-time monitoring of apoptotic cell death. *J. Am. Chem. Soc. 132*, 8309−8315.
(13) Pan, L., He, Q., Liu, J., Chen, Y., Ma, M., Zhang, L., and Shi, J. (2012) Nuclear-targeted drug delivery of TAT peptide-conjugated monodisperse mesoporous silica nanoparticles. *J. Am. Chem. Soc. 134*, 5722−5725.
(14) Fuente, J., and Berry, C. C. (2005) Tat peptide as an efficient molecule to translocate gold nanoparticles into the cell nucleus. *Bioconjugate Chem. 16*, 1176−1180.
(15) Agasti, S. S., Chompoosor, A., You, C., Ghosh, P., Kim, C. K., and Rotello, V. M. (2009) Photoregulated release of caged anticancer drugs from gold nanoparticles. *J. Am. Chem. Soc. 131*, 5728−5729.
(16) Angelos, S., Yang, Y., Khashab, N. M., Stoddart, J. F., and Zink, J. I. (2009) Dual-controlled nanoparticles exhibiting AND logic. *J. Am. Chem. Soc. 131*, 11344−11346.
(17) Zhu, Y., and Fujiwara, M. (2007) Installing dynamic molecular photomechanics in mesopores: a multifunctional controlled-release nanosystem. *Angew. Chem., Int. Ed. 46*, 2241−2244.
(18) Mal, N. K., Fujiwara, M., and Tanaka, Y. (2003) Effects of household dynamics on resource consumption and biodiversity. *Nature 421*, 350−553.
(19) Vivero-Escoto, J. L., Slowing, I. I., Wu, C., and Lin, V. S. Y. (2009) Photoinduced intracellular controlled release drug delivery in human cells by gold-capped mesoporous silica nanosphere. *J. Am. Chem. Soc. 131*, 3462−3463.
(20) Babin, J., Pelletier, M., Lepage, M., Allard, J., Morris, D., and Zhao, Y. (2009) A new two-photon-sensitive block copolymer nanocarrier. *Angew. Chem., Int. Ed. 48*, 3329−3332.
(21) Park, C., Lim, J., Yun, M., and Kim, C. (2008) Photoinduced release of guest molecules by supramolecular transformation of self-assembled aggregates derived from dendrons. *Angew. Chem., Int. Ed. 47*, 2959−2963.
(22) Lin, Q., Huang, Q., Li, C., Bao, C., Liu, Z., Li, F., and Linyong, Z. (2010) Anticancer drug release from a mesoporous silica based nanophotocage regulated by either a one- or two-photon process. *J. Am. Chem. Soc. 132*, 10645−10647.
(23) Knezevic, N., Trewyn, B. G., and Lin, V. S.Y. (2011) Functionalized mesoporous silica nanoparticle-based visible light responsive controlled release delivery system. *Chem. Commun. 47*, 2817−2819.
(24) Knezevic, N., Trewyn, B. G., and Lin, V. S.Y. (2011) Light- and pH-responsive release of doxorubicin from a mesoporous silica-based nanocarrier. *Chem.—Eur. J. 17*, 3338−3342.
(25) Liu, G., and Dong, C. M. (2012) Photoresponsive poly(S-(o-nitrobenzyl)-L-cysteine)-b-PEO from a L-cysteine N-carboxyanhydride monomer: synthesis, self-assembly, and phototriggered drug release. *Biomacromolecules 13*, 1573−1583.
(26) Gou, X., and Szoka, F. C., Jr. (2003) Chemical approaches to triggerable lipid vesicles for drug and gene delivery. *Acc. Chem. Res. 36*, 335−341.
(27) Liu, Y. C., Ny, A. L. M. L., Schmidt, J., Talmon, Y., Chmelka, B. F., and Lee, C. T., Jr. (2009) Photo-assisted gene delivery using light-responsive catanionic vesicles. *Langmuir 25*, 5713−5724.
(28) Jana, A., Devi, K. S. P., Maiti, T. K., and Singh, N. D. P. (2012) Perylene-3-yl methanol: fluorescent organic nanoparticles as a single-component photoresponsive nanocarrier with real-time monitoring of anticancer drug release. *J. Am. Chem. Soc. 134*, 7656−7659.
(29) Russo, P. L., Wozniak, A. J., Polin, L., Capps, D., Leopold, W. R., Werbel, L. M., Biernat, L., Dan, M. E., and Corbett, T. H. (1990) Antitumor efficacy of PD115934 (NSC 366140) against solid tumors of mice. *Cancer Res. 50*, 4900−4905.
(30) Mikata, Y., Mogami, K., Kato, M., Okura, I., and Yano, S. (1997) Synthesis, characterization, interaction with DNA, and antitumor activity of a cis-dichloroplatinum(II) complex linked to an intercalator via one methylene chain. *Bioorg. Med. Chem. Lett. 7*, 1083−1086.
(31) Agorastos, N., Borsig, L., Renard, A., Antoni, P., Viola, G., Spingler, B., Kurz, P., and Alberto, R. (2007) Cell-specific and nuclear targeting with [M(CO)3]+(M = 99mTc, Re)-based complexes conjugated to acridine orange and bombesin. *Chem.—Eur. J. 13*, 3842−3852.
(32) Zelenka, K., Borsig, L., and Alberto, R. (2011) Metal complex mediated conjugation of peptides to nucleus targeting acridine orange: A modular concept for dual-modality imaging agents. *Bioconjugate Chem. 22*, 958−976.
(33) Valu, K. K., Gourdie, T. A., Boritzki, T. J., Gravatt, G. L., Baguley, B. C., Wilson, W. R., Wakelin, L. P. G., Woodgate, P. D., and Denny, W. A. (1990) DNA-directed alkylating agents. 3. Structure-activity relationships for acridine-linked aniline mustards: consequences of varying the length of the linker chain. *J. Med. Chem. 33*, 3014−3019.
(34) (a) Jana, A., Saha, B., Karthik, S., Barman, S., Ikbal, M., Ghosh, S. K., and Singh, N. D. P. (2013) Fluorescent photoremovable precursor (acridin- 9-ylmethyl)ester: synthesis, photophysical, photochemical and biological applications. *Photochem. Photobiol. Sci. 12*, 1041−1052. (b) Piloto, M., Hungerford, G., Costa, S. P. G., and Gonçalves, M. S. T. (2013) Acridinyl methyl esters as photoactive precursors in the release of neurotransmitter amino acids. *Photochem. Photobiol. Sci. 12*, 339−347.
(35) Suzuki, H., and Tanaka, Y. (2001) An unusually acidic methyl group directly bound to acridinium cation. *J. Org. Chem. 66*, 2227−2231.
(36) Zhuang, H. B., Tang, W. J., Yu, J. Y., and Song, Q. H. (2006) Acridin-9-ylmethoxycarbonyl (amoc): a new photochemically removable protecting group for alcohols. *Chin. J. Chem. 24*, 1465−1468.
(37) Mikata, Y., Mogami, K., Kato, M., Okura, I., and Yano, S. (1997) Synthesis, characterization, interaction with DNA, and antitumor activity of a cis-dichloroplatinum(II) complex linked to an intercalator via one methylene chain. *Bioorg. Med. Chem. Lett. 7*, 1083−1086.
(38) Ahmad, B., Parveen, S., and Khan, R. H. (2006) Effect of albumin conformation on the binding of ciprofloxacin to human serum albumin: a novel approach directly assigning binding site. *Biomacromolecules 7*, 1350−1356.
(39) Schumacher, M. A., Piro, K. M., and Xu, W. (2010) Insight into F plasmid DNA segregation revealed by structures of SopB and SopB-DNA complexes. *Nucleic Acids Res. 38*, 4514−4526.
(40) Schüttelkopf, A. W., and Aalten van, D. M. F. (2004) PRODRG: a tool for high-throughput crystallography of protein-ligand complexes. *Acta Crystallogr. D60*, 1355−1563.
(41) Brooks, R., Brooks, C. L., III, Mackerell, A. D., Nilsson, L., Petrella, R. J., Roux, B., Won, Y., Archontis, G., Bartels, C., Boresch, S., Caflisch, A., Caves, L., Cui, Q., Dinner, A. R., Feig, M., Fischer, S., Gao, J., Hodoscek, M., Im, W., Kuczera, K., Lazaridis, T., Ma, J., Ovchinnikov, V., Paci, E., Pastor, R. W., Post, C. B., Pu, J. Z., Schaefer, M., Tidor, B., Venable, R. M., Woodcock, H. L., Wu, X., Yang, W., York, D. M., and Karplus, M. (2009) CHARMM: The biomolecular simulation program. *J. Comput. Chem. 30*, 1545−1614.
(42) Morris, G. M., Goodsell, D. S., Huey, R., and Olson, R. (1996) Distributed automated docking of flexible ligands to proteins: parallel applications of AutoDock 2.4. *J. Comput.-Aided Mol. Des. 10*, 293−304.
(43) DeLano, W. L. *The PyMOL Moleclar Graphics System*; DeLano Scientific: San Carlos, CA, 2004; http://pymol.sourceforge.net/.
(44) Rajendran, A., and Nair, B. U. (2006) Unprecedented dual binding behaviour of acridine group of dye: A combined experimental and theoretical investigation for the development of anticancer chemotherapeutic agents. *Biochim. Biophys. Acta 1760*, 1794−1801.
(45) Chakraborty, B., Singha Roy, A., Dasgupta, S., and Basu, S. (2010) Magnetic field effect corroborated with docking study to explore photoinduced electron transfer in drug-protein interaction. *J. Phys. Chem. A 114*, 13313−13325.